Porous Solids from Layered Clays by Combined Pillaring and Templating Approaches

H. Y. Zhu,*,† Z. Ding,‡ and J. C. Barry§

Department of Chemical Engineering, Centre for Microscopy and Microanalysis, The University of Queensland, St Lucia QLD 4072, Australia, and School of Physical and Chemical Science, Queensland University of Technology, Brisbane 4000, Australia

Received: December 10, 2001; In Final Form: July 22, 2002

The pore structure formation in bentonite, pillared with a mixed sol of silicon and titanium hydroxides and treated subsequently with quaternary ammonium surfactants, is investigated. The surfactant micelles act as a template, similar to their role in MCM41 synthesis. Because both the surfactant micelles and the sol particles are positively charged, it is greatly favorable for them to form meso-phase assembles in the galleries between the clay layers that bear negative charges. Besides, the sol particles do not bond the clay layers strongly as other kinds of pillar precursors do, so that the treatment with surfactants can result in radical structure changes in sol-pillared clays. This allows us to tailor the pore structure of these porous clays by choice of surfactant. The surfactant treatment also results in profound increases in porosity and improvement in thermal stability. Therefore, the product porous clays have great potential to be used to deal with large molecules or at high operating temperatures. We also found that titanium in these samples is highly dispersed in the silica matrix rather than existing in the form of small particles of pure titania. Such highly dispersed Ti active centers may offer excellent activities for catalytic oxidation reactions such as alkanes into alcohols and ketones.

Introduction

Pillaring layered clays with inorganic particles to create a microporous system in the galleries between the clay layers was first proposed in the late 70s.[1−5] The preparation utilizes the peculiar properties of some layered clays: swelling and ion exchange of the interlayer cations.[6] When dispersed in water, the layered clays swell because of hydration of the interlayer cations which act as counterions to balance the negative charges of clay layers. Therefore, species with positive charges in aqueous solutions (the pillaring solution) can be intercalated into the interlayer space by an ion exchange process. Upon heating to above 673 K, the intercalated species undergo dehydration and dehydroxylation and are converted to oxide pillars propping the clay layers apart.[7] A stable micropore system is thus obtained.[5] The pore openings of pillared interlayered clays (PILCs) vary from 0.4 to 2.0 nm, depending on the type of pillars.[8,9] The pore volume and specific surface area are also pillar-dependent, and generally very large, rendering the final pillared clays as excellent candidates for adsorbents and catalyst supports.

Template synthesis of mesoporous molecular sieves of silica or aluminosilicate was first reported in the early 1990s,[10,11] and has attracted a great research interest in recent years.[12] In this novel approach, surfactant (quaternary ammonium salts) in an aqueous medium forms micelles that orient into a well-defined structure. The added silica source is condensed around the micelles forming a silica matrix embedded with organic templates.[10] Alternatively, the surfactant micelles are intercalated between thin layers of kanemite and the silicate layers bend in order to have close contact with the micelles.[11] The templates are removed normally by calcination to create a network of pores that mimic the size and shape of the template. The advantages of this approach are that the pore volume is controlled by the volume fraction of the template constituents, and pore size is controlled by the size of the surfactant micelles. Solids with uniform mesoporous structure and large pore volumes can be obtained by the templating approach.

Recently, efforts have also been made to create a mesoporous system in the galleries between the layers of clays with the templating approach. Galarneau et al reported a successful synthesis of mesoporous solids from layered clays using quaternary ammonium surfactants as template agents.[13] Layered clays were first intercalated with surfactants. These clay layers remain as flat plates because of their better rigidity. Tetraethoxide orthosilicate (TEOS) was then allowed to hydrolyze and condense surrounding the surfactants in the galleries. An open-framework of silica formed in the galleries after removal of the surfactants by heating. In the product solids, part of the pore walls are clay layers.

Actually, there is another approach to create a mesoporous structure in the galleries between the clay layers, reported by Takahama et al.[14] A treatment of montmorillonite intercalated with sol particles of mixed hydroxides of silicon and titanium with octadecyltrimethylammonium (OTMA) resulted in a significant increase in pore volume of the product. They suggested that OTMA molecules diffuse into the interlayer region, resulting in the rearrangement of pillars and the expansion of interlayer space. The subsequent calcination at 773 K burns off the organic compound, leaving enlarged pores in the pillared clay product. However, more experimental evidence is needed to clarify the mechanism of the treatment. One may also raise a question if treatment of the sol pillared clay with other organic ammonium cations i.e., other than OTMA works. This is a concern of significant importance because the choice

* To whom correspondence should be addressed. Phone: 61 7 3365 9058. Fax: 61 7 3365 4199. E-mail: hyzhu@cheque.uq.edu.au.

† Department of Chemical Engineering, The University of Queensland.

‡ School of Physical and Chemical Science, Queensland University of Technology.

§ Centre for Microscopy and Microanalysis, The University of Queensland.

10.1021/jp014463i CCC: $22.00
Published on Web 10/10/2002

of organic ammonium of different molecular sizes may strongly influence the pore size of the solid product as observed in the synthesis of M41 materials, providing opportunities for pore-structure tailoring of sol-pillared clays. Moreover, we find that the effect of pore enlargement by surfactant treatment is unique and can be observed only in the sol-pillared clay, but not in clays pillared with other oxide particles. During last two decades, the potential application of pillared clays as catalysts or catalyst supports for numerous chemical reactions has been attempted.[15] In general, better acidic characteristic, larger specific surface area, pore volume, and pore size are required for catalysis purpose. It is highly possible that the sol intercalated clays treated with surfactant possess these required properties and are a potential advance for this purpose. Therefore a comprehensive characterization of these solids is of great significance. For instance, the existence of titanium in sol pillared clays is also of particular interest. In SiO_2-TiO_2 sol-pillared clay, titanium is introduced to make the sol particles positively charged so that they can be cation-exchanged with the cations present between the silicate layers of the clays.[14] The SiO_2 sol particles resulting from hydrolysis of TEOS are neutral or negatively charged. By mixing with a small amount of TiO_2, one could obtain sol particles with positive charges. It should be also noted that the existence of titanium, even in a small quantity, can significantly enrich the properties and functions of these clay materials. For example, it is known that anatase is very active for the photooxidation of organic compounds in water.[16,17] Montmorillonite clay intercalated with TiO_2 of anatase phase has also been found to be an active catalyst for such a reaction.[18] Besides, the framework-isolated Ti(IV) sites are thought to be the active sites in Ti-silicalite for the catalytic oxidation of alkanes into alcohols and ketones using H_2O_2 as oxidant.[19−22] However, anatase phase is inactive for these reactions. These facts suggest that the location and structure of the incorporated titanium in the sol-pillared clays play very important roles in their catalytic activities.

In the present study, a systematic investigation into the synthesis and characterization of the sol-pillared clay treated with different surfactants is conducted. A comprehensive comparison of their characteristics with those of MCM41 provides insights into the pore structure formation of the sol-pillared clays in the presence of the surfactants. The state of titanium in these solids is also investigated by spectroscopic techniques. The fundamental information derived from this study is important in developing catalysts or adsorbents of tailorable pore structure and desired active sites from layered clays.

Experimental Section

Preparation. Sodium bentonite was supplied by Commercial Minerals Ltd., Australia, and used as the starting clay material. Over 90% of the bentonite powder has particle size < 2 microns and its cation exchange capacity (CEC) is 75 meq/100 g of clay.

The sol-pillared clay was prepared following the procedure of Yamanaka et al.[23] The sol solution of silicon hydrate was prepared by mixing TEOS, $Si(OC_2H_5)_4$, 2 M HCl and ethanol in a ratio of 41.6 g:10 mL:12 mL at room temperature. Titanium tetra-isopropoxide $Ti(OC_3H_7)_4$ was hydrolyzed in a 1 M HCl solution and the molar ratio of HCl to $Ti(OC_3H_7)_4$ was about 4. The resulting slurry was peptized to a clear sol solution by continuous stirring for 3 h at room temperature. The two sol solutions were then mixed and stirred for 30 min at room temperature. Subsequently, the mixture was added into a 1% (w/w) suspension of clay under vigorous stirring such that a mixing ratio of 30:3:1 for Msi (mol)/M_{Ti}(mol)/CEC equivalent of the clay was established. The slurry was stirred for 6 h to allow sufficient intercalation, and then the solid was separated by centrifugation. The wet cake was divided into equal portions, and each portion was mixed with a template, quaternary ammonium bromide $[CH_3(CH_2)_{n-1}\ N(CH_3)_3Br]$, respectively, by stirring for about 2 h, except for one portion left as a reference, where n in the above formula denotes the number of carbon atoms in the alkyl chain of the surfactant. Surfactants with n =12, 14, 16 and 18 were used in this work. The ratio of surfactant to clay, expressed in moles of surfactant to CEC of the clay, was 5:3. The resultant mixture of clay and surfactant was transferred into an autoclave and kept in an oven at 373 K for 3 d. The wet cake was then recovered by filtration and washed with water to Cl^- ions free. The solid was dried at room temperature and calcined at 773 K for 4 h. The calcined products was labeled sol-PILB−Cn. Without being mixed with any surfactant and subjected to treatment at 373 K, the portion of the wet cake as reference was directly washed, dried, and calcined under the same conditions as those for other samples and termed as sol-PILB.

For comparison, a series of MCM41 samples were prepared with the same surfactants as templates. The surfactant was dissolved in a solution of NaOH first, and then a desired amount of silica fume (from Aldrich, 99% of silica) was dispersed in the solution under vigorous stirring. The molar ratio in the mixture was: 3.6 Na_2O:30 SiO_2:5.1 surfactant:700 H_2O. The resultant cream-like slurry was transferred into an autoclave for aging under the same condition as for the mixtures of intercalated clay and surfactants. The white solids were recovered and washed, dried and calcined using the same procedures as those for the sol-PILB−Cn samples. They were labeled MCM41-Cn.

Characterization. The chemical composition of the samples was analyzed using an atomic absorption spectrometer (AAS). The fusion method was used to prepare the samples and standards.[24] X-ray diffraction (XRD) patterns of sample powder were recorded on a Philips PW 1840 powder diffractometer with cobalt K_α radiation at 40 kV and 20 mA and a nickel filter. Transmission electron microscopy (TEM) images were taken with a JEOL 2010 microscope on powder samples deposited onto a copper micro-grid.

N_2 adsorption/desorption isotherms were measured at liquid nitrogen temperature using a gas sorption analyzer (Quantachrome, NOVA 1200). The samples were degassed at 573 K for 3 h prior to the adsorption measurement. The specific surface area was calculated by the BET equation,[25] and the external and surface area of framework pores was determined with the t-plot method of Lippens and De Boer.[26]

The adsorption of water vapor by the samples was measured at 293 K using a gravimetric measurement rig with quartz springs as the microbalance elements. About 80−90 mg of calcined sample was degassed at 473 K overnight in a vacuum prior to the adsorption measurement. The adsorption behavior at low pressures of vapor indicates the hydrophobicity of the samples under test.

Thermogravimetric analysis (TGA) of the samples was performed on Shimadzu TGA-50. About 10 mg of solid before calcination was loaded on a platinum pan and heated from room temperature to 1073 K at a heating rate of 5 K/min in an air flow of 80 mL/min.

Fourier transform infrared (FTIR) spectra of the samples were recorded by a Perkin-Elmer 2000 FTIR spectrometer. Specimens for the measurements were prepared by mixing the sample powder dried at 573 K for 3 h with KBr and pressing the mixture into pellets. The weight ratio of sample to KBr was about 2:100.

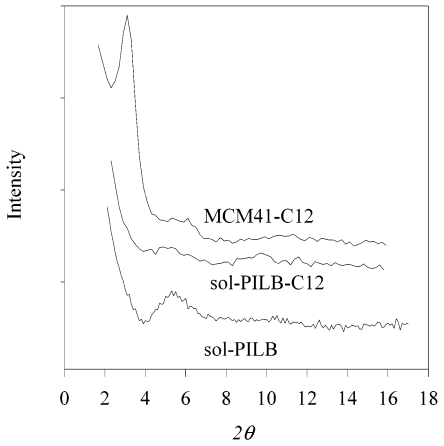

Figure 1. XRD patterns of (from bottom to top) sol-PILB, sol-PILB−C12, and MCM41−C12.

Spectra were acquired in a wavenumber range between 500 and 4000 at 2 cm^{-1} resolution and averaged over 100 scans.

Temperature programmed desorption of pyridine (PTPD) was conducted using Shimadzu TGA-50. The calcined samples were heated at 573 K overnight and were then equilibrated with pyridine vapor at 323 K overnight. About a 10 mg portion of the pyridine-saturated solid was heated linearly at various rates, from 1K/min to 10 K/min, to 773 K in helium flow of 80 mL/min. The weight loss as the temperature rises is due to desorption of pyridine from acidic sites on the sample surface. The first derivative of weight loss with respect to temperature (DTG) was plotted against temperature as the TPD profiles.

Diffuse reflectance spectra in the UV−vis range (DR−UV/VIS), 200−900 nm, were recorded using JASCO 550 UV/VIS spectrophotometer equipped with a JASCO ISV-469 integrating sphere attachment. The absolute remittance R_∞ from sample was measured.

Results

XRD Patterns and TEM Images. A broad peak at about 5.3° is the most obvious one on the XRD pattern of sol pillared clay after calcination (Figure 1), which reflects the short-range aggregation of clay sheets. The long-range aggregation of clay layers could be in a poor order. The corresponding basal spacing was thus estimated to be 1.94 nm and the free spacing, 0.98 nm (= 1.94 nm − 0.96 nm, where 0.96 nm is the thickness of a single silicate layer of montmorillonite clay). This result is consistent with what we observed from TEM images. Part of this sample exhibits a basal spacing about 1.9 nm (Figure 2a), which is responsible for the diffraction at about 5.3°. But in other parts, the spacing is larger and varies from 2.4 to 2.9 nm (Figure 2b). Occelli et al.[27] reported a similar XRD pattern for montmorilonite pillared with the same sol particles. Yamanaka et al.[23] and Choy et al.[28] observed a peak at lower angles, which corresponds to the free spacing of about 3 nm. Their secondary diffraction is close to the peak we observed at about 5.3°. However, they also argued that the 3-nm free spacing could not represent the size of the preponderant portion of pores in the pillared clay. Adsorption of nitrogen and organic vapor by the sol-pillared clay indicates that most of the surface area and pore volume of this solid arises from micropores (pore size < 2 nm).[23] The sharp diffraction peaks are characteristic of the XRD patterns of MCM41 sample,[10−12] reflecting the uniform pore structure formed by the templating mechanism. The XRD pattern of MCM41-C12 sample is also given in Figure 1.

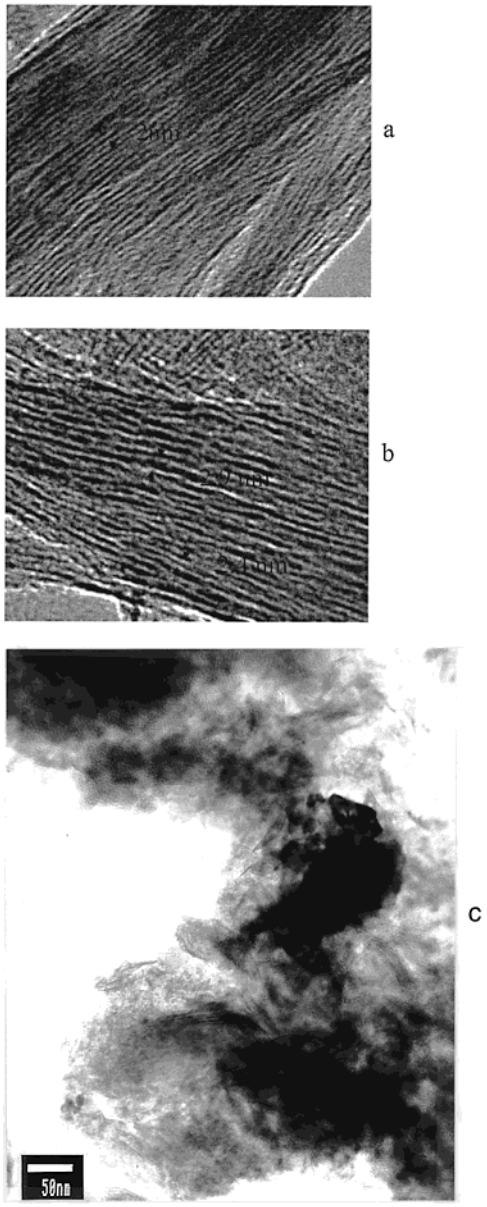

Figure 2. TEM images of sol-PILB (a and b) and sol-PILB−C16 (c).

The pattern of sol-PILB−C12 sample is illustrated in Figure 1 as representative of the sol-PILB−C*n* samples. Although both pillaring and templating approaches lead to ordered structures, no obvious peaks were observed in the XRD patterns of sol-PILB−C*n* samples, which were obtained by combining the two approaches. The XRD patterns suggest that these samples have a poor long-range order in their structures. This is supported by the TEM image of sol-PILB−C16 shown in Figure 2c.

The wires of uniform thickness of about one nanometer in the image of Figure 2b are believed to be the edges of the clay layers. One can see bundles of several clay platelets in the figure. The separation space between the layers in sol-PILB−C16 is irregular, and in a range of several nanometers. Clearly, the layered sheets of bentonite are intercalated, but there is no long-range order in the arrangement of these layers. Therefore, the sample cannot give a sharp XRD peak as the conventional pillared clays. Moreover, most separations between the clay layers in Figure 2c are obviously larger than those in the parent sample sol-PILB (Figure 2, a and b). For the intercalated structures, the pore size is comparable to the interlayer space.[1−5] The detailed information of the pore structure in these samples

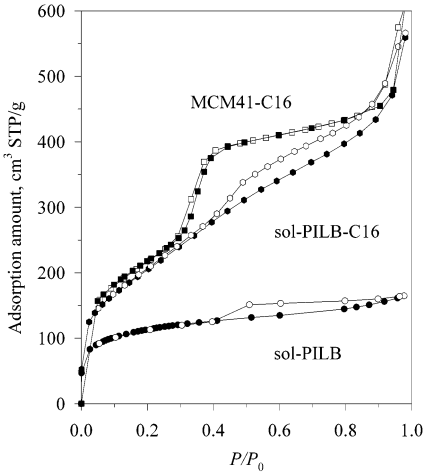

Figure 3. N_2 ads-desorption isotherms of sol-PILB, sol-PILB−C16, and MCM41−C16 samples. Solid symbols represent adsorption and empty ones, desorption.

has to be derived from nitrogen ads-desorption data as discussed below.

Nitrogen Adsorption. N_2 adsorption/desorption isotherms of sol-PILB (the reference sample), sol-PILB−C16 and MCM41-C16 are compared in Figure 3. The last two are the representatives of sol-PILB−C*n* and MCM41-C*n* samples, respectively.

Distinct differences in the shape of the isotherms are observed (Figure 3). The sol-PILB is mainly of the character of Type I, generally observed for microporous solids, according to the B. D. D. T. classification,[29] except for an obvious hysteresis. Adsorption below the relative pressure of 0.4 accounts for most of the overall adsorption amount, indicating a large number of micropores existing in this solid.[25] In contrast, the adsorption of sol-PILB−C*n* sample increases steeply in high relative pressure region. The treatment with surfactant results in a significant increase in the porosity of the clay and thus the adsorption capacity. The adsorption of sol-PILB−C16 is comparable to that of MCM41-C16, and remarkably larger than that of sol-PILB. This indicates that the templating mechanism which works in the synthesis of MCM41 materials[10−12] may also be true in the treatment of the sol pillared clay with surfactants. Nevertheless, there are appreciable differences between the isotherms of sol-PILB−C*n* and MCM41-C*n*. The isotherm of sol-PILB−C16 can be ascribed to Type IV isotherms,[25,29] and there is an inclined hysteresis for sol-PILB−C16. There is no evident hysteresis on the isotherm of MCM41-C16. The adsorption behavior of MCM 41 is related to the uniform cylindrical pores in their framework.[10−12,30−35] The obvious hysteresis observed on the isotherms of sol-PILB−C16 is attributed to the existence of mesopores with irregular geometry.

Important pore structure parameters such as the specific surface areas, pore volumes, and mean hydraulic radius of the framework pores (which is derived from the ratio of the volume to surface area of these pores) can be calculated using the data of N_2 ads-desoprtion.[25,34] The results are summarized in Table 1.

The BET surface areas and total pore volume of the sol-PILB−C*n* samples are much higher than those of the parent sol-PILB sample but are closer to those of the MCM41 samples. This is particularly obvious for sol-PILB−C16 and −C18 samples. The pore and surface area parameters of sol-PILB−C16 and MCM41−C16 are very close. The same applies for sol-PILB−C18 and MCM41−C18. As the alkyl chain of the surfactants increases, the surface area and the pore volume of sol-PILB−C*n* samples approach to the corresponding values of the MCM41 samples prepared using the same surfactant as template (Table 1). The treatment with surfactants brings about a radical change in the structures of the intercalated clay, resulting in highly mesoporous solids.

TABLE 1: Specific Surface Area (s. area), Pore Volume (p. vol.), and Mean Hydraulic Radius of the Framework Pores

	overall		framework pores		
samples	s. area (m^2/g)	p. vol. (cm^3/g)	s. area (m^2/g)	p.vol (cm^3/g)	pore radius (Å)
sol-PILB	402.0	0.238	370.7	0.186	9.9
		sol-PILB−C*n*			
−C12	620.4	0.645	395.6	0.211	10.6
−C14	721.4	0.797	440.8	0.257	11.6
−C16	750.2	0.876	475.9	0.331	13.9
−C18	687.7	0.945	403.5	0.331	16.4
		MCM41−C*n*			
−C12	830.7	0.515	722.3	0.386	10.7
−C14	963.8	0.745	764.9	0.524	13.7
−C16	789.8	0.943	668.6	0.536	16.1
−C18	652.6	1.085	475.2	0.450	19.0

The data of N_2 ads-desoprtion are also widely used to derive the pore size distributions (PSD) of porous solids.[25] The conventional methods based on the Kelvin equation are applicable to mesopores but not to micropores. Moreover, for the small mesopores, it has been found that these methods substantially underestimate the pore dimension.[34−36] The Dubinin theory[37] and Horvath- Kawazoe method[38] for deriving PSD of microporous solids are not appropriate for calculating the size and volume of mesopores because the capillary condensation that occurs in mesopores is not taken into account in these methods. Recently, we proposed a method based on an empirical relation.[39] It can be applied over the range 1 nm ≥ pore size ≥ 5 nm. Supermicropores and small mesopores, which are relevant to this study, are included in this pore size range. This method is based on the widely used comparison plots, *t*- and α_s-plots,[26,40] which have been well accepted for estimating the parameters of micropores in porous solids.[25] For solids with substantial pore volume distributed over micropore and small mesopores, our method can give reasonable PSD results. PSDs of all three representative samples, obtained by this method are presented in Figure 4.

According to the PSD of sol-PILB, most of the pore volume is attributed to micropores (pore size below 2 nm). However, the broad PSD also indicates that the pore structure is not uniform. The treatment with the surfactant of an alkyl chain of 16 carbon atoms leads to a shift of the PSD to larger pore sizes. The PSD peaks at about 1.5 nm (assuming a cylindrical pore geometry). It is very close to the peak position in the PSD of MCM41-C16. This fact supports the argument that the templating mechanism similar to that in MCM41 synthesis works in the surfactant treatment of sol-PILB. The PSD of sol-PILB−C16 is much broader than that of MCM41-C16, indicating the irregularity in the pore structure. This is consistent with the evident hysteresis on ads-desorption isotherms, irregular structure in TEM and the featureless XRD patterns for the clay samples.

If the templating mechanism works in the treatment of sol-PILB with surfactant, the size of the mesopores will be directly proportional to the chain length of the quaternary ammonium surfactants. The relation between the mean diameter of the framework pores in sol-PILB−C*n* samples and the chain length of the surfactants, expressed by the number of carbon atoms in the alkyl chain in the surfactants (C*n*), is shown in Figure 5.

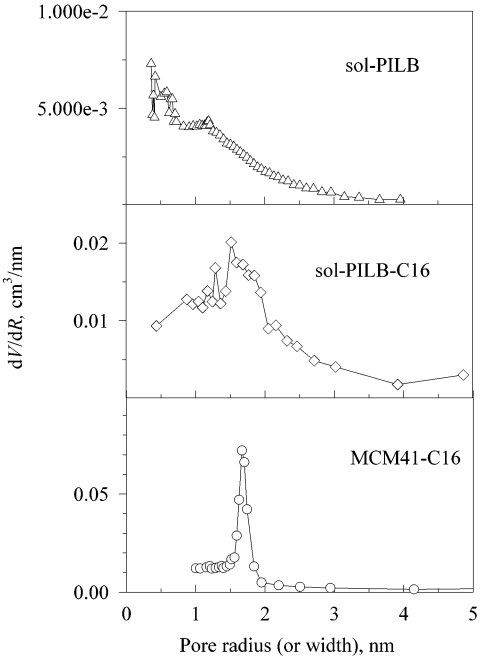

Figure 4. Pore size distribution (PSD) of sol-PILB, sol-PILB−C16, and MCM41−C16.

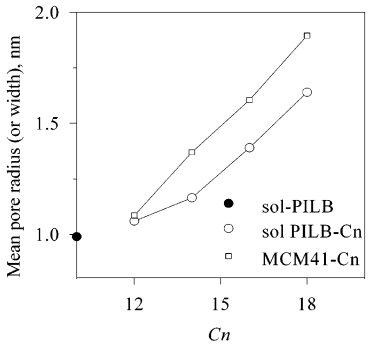

Figure 5. Relation between the mean radius of the framework pores in sol-PILB−Cn samples and C*n*, the number of carbon atoms in the alkyl chain in surfactants.

TABLE 2: Main Chemical Composition of Starting Clay (Bentonite), sol-PILB, and sol-PILB−C*n* Samples

	SiO_2	Al_2O_3	TiO_2	Si/Ti	SiO_2 excess (to Bentonite)	SiO_2 excess (to sol-PILB)
Bentonite	63.67	17.51	<1.97			
sol-PILB	70.39	11.59	9.66	3.89	28.25	
sol-PILB−Cn						
-C12	73.73	9.23	8.83	5.51	36.63	8.38
-C14	75.80	10.05	9.35	4.76	33.48	5.24
-C16	75.10	9.69	9.20	4.79	33.15	4.90
-C18	73.27	9.23	9.10	4.92	33.68	5.43

Such a relation for silica MCM41 samples is also given in this figure for comparison. The pore size of sol-PILB−C*n* samples are generally larger that that of the normal sol-PILB (given on the vertical axis) and increases with C*n*. The relation of the pore dimension with C*n* is very similar to that for MCM41 samples. The results shown in Figure 5 further support that the templating process occurs during the surfactant treatment.

Chemical Analysis. The main compositions of the starting clay, sol-PILB and sol-PILB−C*n* samples, represented as mass percentage of oxides, are summarized in Table 2.

The increase in silica and titanium oxide contents in sol-PILB compared to those in the starting clay, due to the intercalation

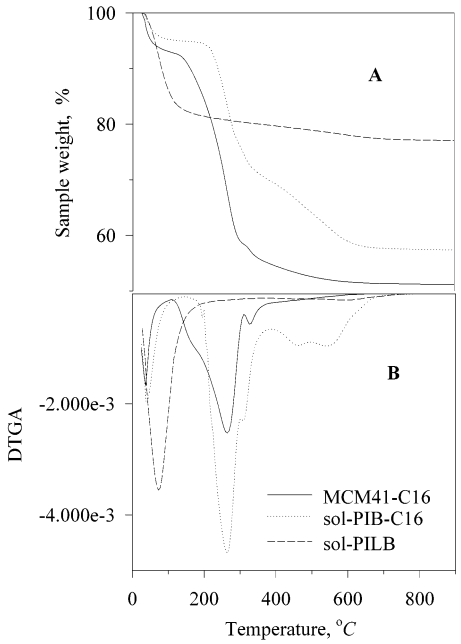

Figure 6. (A) Weight losses of the uncalcined samples when heated to 900 °C in air. (B) differential weight loss curves (DTG).

with the sol particles, is anticipated and consistent with the results reported in the literature.[23,27,28] In addition, the composition of the clay layers should remain unchanged during the pillaring process. Therefore, silica from the clay layers of sol-PILB sample can be calculated with the alumina content of the sample, because the pillaring process causes no change in the ratio of silica to alumina for the clay layers. Thus, the pillar particles account for 28.25 wt % of sol-PILB, as expressed in term of SiO_2 excess to bentonite in Table 2. The silica content of sol-PILB−C*n* samples is slightly higher than that in sol-PILB.

Actually we can rule out the possiblity that the sol-PILB−C*n* samples are mechanical mixture of MCM41 and the clay based on the data in Tables 1 and 2. As seen in Table 2, one gram of sol-PILB−C*n* product contains about 0.67−0.63 g of bentonite clay. The rest is oxide formed from the mixed sol. If the oxides (mainly silica) form a highly porous structure of MCM41 but outside the clay in the form of a mechanical mixture of the oxide and clay, the specific surface area of a mechanical mixture of the oxide and clay should be about 400 m^2/g or lower (The BET specific surface area of bentonite is about 50 m^2/g, and the contribution from 0.63 g of clay to specific surface area should be 31.5 m^2/g; whereas the contribution from 0.37 g of MCM41 pore structure is about 370 m^2/g). This estimated 400 m^2/g for such a structure is far short of the surface area data actually obtained (Table 1), between 620 and 750 m^2/g. This is consistent with the observation in TEM image. A large fraction of oxide particles exist within the galleries between the clay layers.

Thermogravimetric Analysis. Figure 6A shows the weight losses when the uncalcined samples were heated in air up to 900 °C. Figure 6B is the differential weight loss curves (DTG). The results of sol-PILB and MCM41−C16 are also shown. For sol-PILB, the major weight loss, about 15%, occurs below 150 °C, due to dehydration of the pillars. Whereas for MCM41−C16, the weight loss in this temperature region is relatively small, about 7%. The major weight loss for MCM41−C16 occurs between 140 °C and 300 °C, due to the burning off of the template. It is found that this loss increases with the carbon

TABLE 3: Specific Surface Area and Porosity of Samples Heat Treated at 700 and 800 °C

	sol-PILB−C*n*		MCM41−C*n*	
T (°C)	s. area (m^2/g)	volume (FWP) (cm^3/g)	s area (m^2/g)	volume (FWP) (cm^3/g)
		without surfactant (sol-PILB)		
700	358.6	0.177		
800	162.7	0.057		
		−C12		
700	610.4	0.211	816.3	0.302
800	493.4	0.154	317.9	0.102
		−C14		
700	525.9	0.210	722.1	0.391
800	441.7	0.128	694.2	0.311
		−C16		
700	551.4	0.226	669.6	0.380
800	327.3	0.089	594.9	0.282
		−C18		
700	522.3	0.204	158.0	0.063
800	477.8	0.124	143.0	0.062

chain length of the surfactant, being about 28% for MCM-C12 and 37% for MCM41-C16, respectively. Sol-PILB−C*n* samples exhibit a thermal behavior that appears hybrid of those of sol-PILB and MCM41 samples. Sol-PILB−C12 exhibits the largest weight loss below 150 °C among these samples, but the smallest weight loss between 150 and 300 °C. The behavior of this sample is very similar to sol-PILB. As the length of the carbon chain in the surfactant increases, this similarity diminishes. The thermogravimetric behavior of sol-PILB−C16 and sol-PILB−C18 is very similar to the MCM41 samples, with a small weight loss below 150 °C and a very large weight loss between 150 °C and 300 °C.

These results demonstrate the dependence of the properties of sol-PILB−C*n* on the properties of the surfactants which were used to treat the intercalated sol-PILB. The properties of the sample treated with a surfactant of longer carbon chain is closer to those of MCM41, which is consistent with observed trend from the BET surface area and total pore volume, as shown in Table 1.

Thermal Stability. Heating at high temperatures always results in a loss of surface area and collapse of small pores. The surface areas and pore volumes of sol-PILB, sol-PILB−C*n* as well as MCM41−C*n* samples, after calcinations at 700 °C and 800 °C, are given in Table 3.

Smectite clays and their pillared derivatives are generally unstable at above 700 °C.[41] Heating at 800 °C causes serious damage to the clay layers and a complete loss in crystallinity of the layers.[42] For instance, the surface area of sol-PILB drops by about 60%, from 402 m^2/g to 163 m^2/g after heating at 800 °C. However, the pore structures of sol-PILB−C*n* samples exhibit better resistance to the heating at high temperatures. The decrease in surface area is below 40%. After heat treatment at 800 °C, sol-PILB−C*n* samples still have a surface area well above 400 m^2/g. The pore structures of MCM41−C*n* samples also show a superior resistance to heating at high temperatures (Table 3). According to these results, the framework pore of sol-PILB−C*n* should be different from that in sol-PILB, but resembles to a certain extent to that of MCM41.

FTIR Spectra. In Figure 7, FTIR spectra of sol-PILB−C14, sol-PILB, and MCM41−C14 are compared. Absorption bands in the range 3000−3800 cm^{-1} correspond to O−H stretching vibrations, including those of adsorbed water molecules. For sol-PILB and sol-PILB−C*n* samples, a band appears as a shoulder peak at around 3643 cm^{-1}. This is attributed to hydroxyl groups on the surface of clay layers.[43] This band is observed in the FTIR spectra of other pillared clays prepared in this laboratory but not in the spectra of MCM41 samples. The band observed at around 1640 cm^{-1} is assigned to the bending mode of adsorbed water molecules.[44]

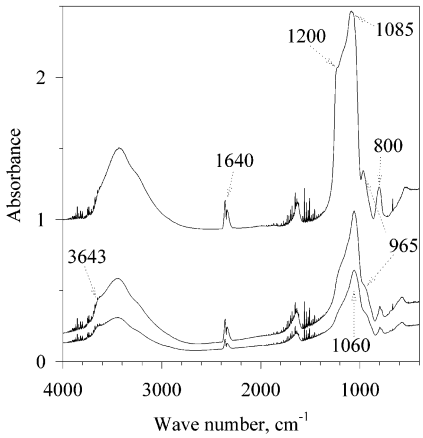

Figure 7. FTIR spectra of the clay samples. From the bottom to top: sol-PILB, sol-PILB−C14 and MCM41−C14.

The absorption bands appearing at around 1085 cm^{-1} with a shoulder at about 1200 cm^{-1} and the band at around 800 cm^{-1} are characteristic of the infrared spectra of silica.[44,45] The band at 1085 cm^{-1} is due to asymmetric Si−O stretching and the one at 800 cm^{-1}, due to symmetric Si−O stretching mode. Nevertheless, it has been observed in the spectra of the layered silicate, like clays, that these bands shift to lower wavenumbers.[43] As can be seen from the spectra of sol-PILB−C*n* and sol-PILB samples, these bands appear at around 1050 and 796 cm^{-1}, respectively. They can be attributed to the stretching modes of the silicate layers in sol-PILB and sol-PILB−C*n* samples.

The absorption band observed between 970 and 920 cm^{-1} is of particular interest. For MCM41 consisting of mainly amorphous silica, a separated peak at around 967 cm^{-1} is observed. For the clay samples, the band appears as a shoulder to the strongest band of asymmetric Si−O stretching at around 1050 cm^{-1}. This band is assigned to the stretching motion of external $Si-O^-$ groups.[44−50] Because the band of asymmetric Si−O stretching shifts to low wavenumbers for clay samples, a shoulder rather than a separate peak is observed. In addition, a bonding form of Si−O−Ti is also the cause of the band in this range.[45,48,49] Contribution from vibration of such a bonding form to this absorption band is possible for the clay samples. This bonding form also gives a hint that titanium exists in a form different from small particles of pure titanium oxide, but probably in a 4-fold coordination or in a distorted five or six coordination in the silica network.[45,48] This argument is further supported by the spectra shown in Figure 8.

Figure 8 shows the FTIR spectra of bentonite clays pillared with alumina (Al−PILB) and with titania (Ti−PILB), sol-PILB−C16 and a commercial titania (Degussa P25) in a region of low wavenumbers, between 1200 and 500 cm^{-1}. The most remarkable feature is that strong absorption bands can be observed in the range 900−600 cm^{-1} for titanium oxide and Ti−PILB. With our results from the XRD measurements in mind, we can conclude that these bands are attributed to the vibration modes of anatase. The absorption bands of sol-PILB−C*n* samples in this region are similar to those for Al−PILB. The characteristic absorption bands for titanium oxide is not observed. This suggests that titanium in these samples is highly

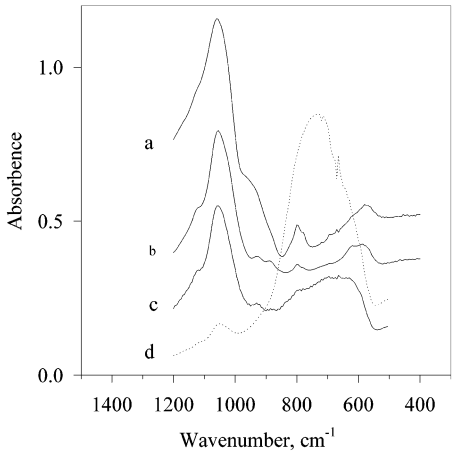

Figure 8. FTIR spectra of four solids in a region of low wavenumbers, between 1200 and 500 cm^{-1}. (a) sol-PILB−C16; (b) bentonite pillared with alunima; (c) bentonite pillared with titania; and d, commercial titania (Degussa P25).

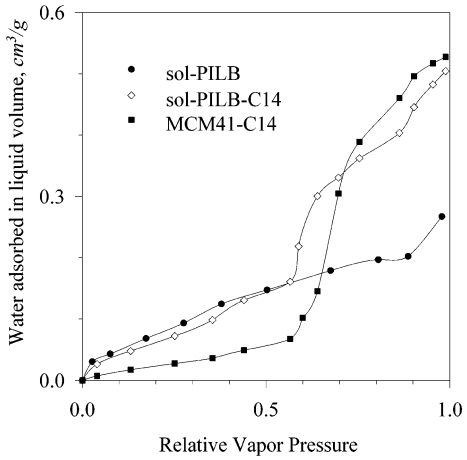

Figure 9. Water adsorption on clay samples.

dispersed in the amorphous silica network (the pillars), not forming particles of TiO_2. This situation could be similar to titania in SiO_2-TiO_2 glass. This conclusion will be further supported by the results of DR−UV−vis spectra as discussed later.

Water Adsorption. The behavior of water adsorption by a solid is associated with the surface polarity and pore structure of the solid. Hydrophilic surfaces are of a strong polarity, which exhibit strong adsorption of the polar molecules of water at low vapor pressures. Water adsorption by sol-PILB and sol-PILB−C14 and MCM41−C14 are shown in Figure 9.

Very strong adsorption at low vapor pressures are observed for the two clay samples, compared to that of MCM41-C14. It is noted that there is a large amount of micropores in the clay samples (Figure 4). In narrow micropores, the adsorptive molecules are subjected to strong attractive forces. At low vapor pressures, the adsorption by sol-PILB is the strongest although the specific surface area of sol-PILB is substantially lower than that of sol-PILB−C14 and that of MCM41-C14. This is attributed to the preponderance of the micropores in this sample. This result is in good agreement with that reported by Malla and Komarneni.[51] In addition, the existence of titanium could enhance surface polarity, and thus, the adsorption of the polar molecules on the surface. The surfaces of the clay samples can be much more hydrophilic than that of MCM41-C14 due to this reason.

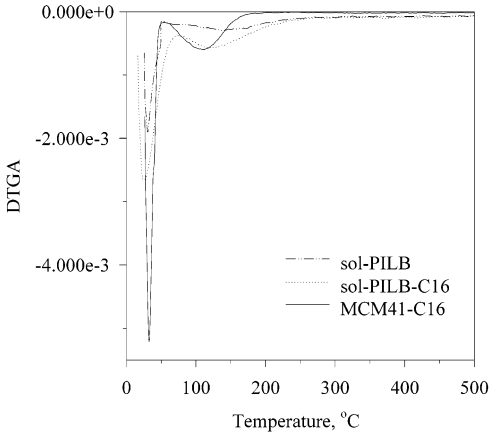

Figure 10. Pyridine TPD profiles for clay samples.

The steep increase in adsorption above a relative vapor pressure of 0.5 is usually observed for samples prepared with surfactant templates, sol-PILB−C*n* and MCM41−C*n*. At these pressures, capillary condensation in the framework mesopores takes place, filling the mesopores. Large volumes of the framework mesopores with similar pore dimensions in these samples result in the steep increase in adsorption. This characteristic is consistent with the results of pore structural parameters derived from nitrogen adsorption data.

TPD of Pyridine. In Figure 10, the results of pyridine-TPD are illustrated. The curves are expressed as the first derivative of weight loss (DTGA) vs temperature.

Two desorption peaks are observed on all samples. This means that there are two groups of surface sites that are of quite different acid strengths. The low temperature peak corresponds to the sites of weak acidity. This peak appears at almost the same temperature for all three samples, and these sites are mostly hydrogen bonded SiOH groups. The temperature for the second peak varies from sample to sample, in the following order:

MCM41−C*n* < sol-PILB−C*n* < sol-PILB.

The desorption temperature should be indicative of the activation energy required for desorption. If a sample has strong acid sites, then the base molecules of pyridine will be held strongly on these sites until liberated at higher temperature. As a consequence, the desorption peak occurs at higher temperatures. Therefore, the above sequence is also the order for the strength of surface acidity of these samples. We can calculate the activation energy of desorption from the sites of second group using the equation proposed by Cveanovic and Amenomiya[52]

$$2 \ln T_m - \ln \beta = \frac{E_d}{RT_m} + \ln \frac{E_d}{AR} \qquad (1)$$

where T_m is the temperature at which the second peak appears (K), β is the heating rate (K/min) during desorption, E_d is the activation energy of desorption, R is the gas constant (8.314 kJ/mol), and A is the preexponential factor. By plotting ($2\ln T_m - \ln\beta$) against ($1/T_m$), we can obtain the value of E_d/R. The energy E_d is 59.8 kJ/mol for MCM41−C16 and 66.4 kJ/mol for sol PILB−C16. The greater value of E_d for sol-PILB−C*n* suggests that they have a stronger surface acidity than the MCM41 samples. This gives a quantitative explanation to the observation that desorption from sol-PILB−C*n* extends to higher temperature with a substantial larger amount of pyridine compared to the desorption from MCM41.

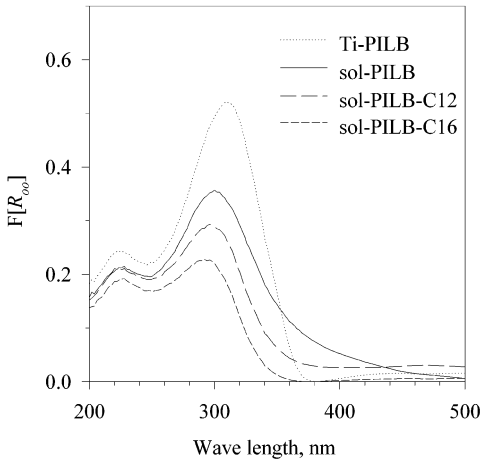

Figure 11. DR−UV−vis spectra of clays expressed in Kubelka−Munk function $F(R_\infty)$ against wavelength.

DR−UV−Vis Spectra. Relative remittance quantity R'_∞

$$R'_\infty = R_\infty(\text{sample})/R_\infty(\text{standard}) \quad (2)$$

is used to calculate the Kubelka−Munk function defined as $F(R_\infty)$[53]

$$F(R_\infty) = (1 - R'_\infty)^2/2R'_\infty. \quad (3)$$

Figure 11 shows the curves of $F(R_\infty)$ against wavelength for four samples. For clarity, two curves of sol-PILB−C*n* samples are given, together with the curves of sol-PILB and Ti-PILB. Titania pillars in Ti-PILB were from hydrolysis of titanium tetraisopropoxide. A sample of porous clay heterostructure,[54] which contains bentonite and silica resulting from hydrolysis of TEOS, was used as the reference.

Two peaks can be observed on these curves. A weaker one is at about 225 nm for all samples. The position of the intense peak is different from sample to sample. The wavelength of this peak for sample follows the order:

sol-PILB−C*n* < sol-PILB < Ti-PILB.

This peak appears at about 292 nm for sol-PILB−C16 and at 310 nm for Ti−PILB. Moreover, for sol-PILB−C*n* samples, as *n* (the length of alkyl chain) increases, this peak shifts to short wavelengths (288 nm for sol-PILB−C18 and 296 nm for sol-PILB−C12). The values of function $F(R_\infty)$ for these samples show the same trend: decreasing from Ti=PILB to sol-PILB−C18. The shoulder at 225 nm is assigned to isolated Ti atoms with 6-fold coordination.[49,55] According to Petrini et al.,[55] the peak of 270 nm arises from partially polymerized 6-coordinated Ti species, which contain Ti−O−Ti bonds and exists in the amorphous silica matrix. This further confirms the bond involving Si and Ti causing the absorption band at 960 cm^{-1} in FTIR spectra. Anatase is regarded as the source for the peak at about 320 nm.[49] Therefore, the strong peak at 310 nm for Ti−PILB is mainly due to anatase phase whose existence has been confirmed by XRD pattern as shown earlier. However, titanium in sol-PILB and sol-PILB−Cn samples exists in partially polymerized and partially isolated Ti species according to Figure 11. The shift to short wavelengths as *n* increases could be due to a decrease in the polymerization degree of Ti species.

The function $F(R_\infty)$ is directly proportional to the concentration of the species responsible for the peak.[57] The decreasing trend of $F(R_\infty)$ should reflect that Ti content in these samples decreases in the same order. The decrease in Ti content can be also related to the porosities of these samples. The pore volumes

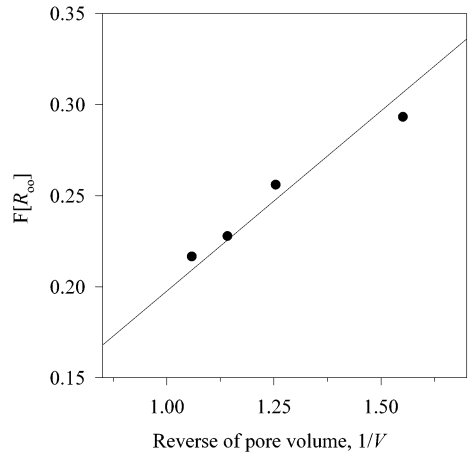

Figure 12. Relation between $F(R_\infty)$ of the peak at about 290 nm and 1/V for sol-PILB−C*n* samples.

of sol-PILB−C*n* samples increase with *n*, as shown in Table 1. It is also noted that the pore volume follows the order:

Ti-PILB < sol-PILB < sol-PILB−C*n*.

The density of a sample with a larger pore volume is lower so that the concentration of titanium per unit volume will be lower. In the measurements of DR−UV−vis spectra, the volume of the sample used was almost the same. Figure 12 shows a linear relation between $F(R_\infty)$ of the peak at about 290 nm and (1/V) for sol-PILB−C*n* samples which have similar Ti/Si ratios. The sol-PILB deviates from this linear relation, and we note that Ti/Si ratio for this sample is obviously higher (Table 2).

Discussion

Formation of Mesostructures in Intercalated Clays upon Surfactant Treatment. When the work of Takahama et al.[14] was published, the mechanism of micelles of the surfactant molecules acting as template for the formation of uniform mesostructures had not been recognized. In the present study, a systematic investigation on the surfactant treatment of sol-particle intercalated clays and comparison of the resultant clay solids with MCM41 prepared using the same series of surfactants are conducted.

The results presented in this work strongly support that the surfactant micelles act as templates in the surfactant treatment of sol-PILB in a manner similar to MCM41 synthesis. Large and irregular interlayer space between the clay layers is observed (Figure 2). The peak in PSD of these surfactant treated samples is observed at pore sizes close to that in the corresponding MCM41, and it shifts to larger pore sizes as the length of alkyl chain of surfactants increases, the same trend as that observed in MCM41 samples. Similarities are also found in sol-PILB−C*n* and corresponding MCM41 samples in thermogravimetric behavior, specific surface areas and pore volumes, and thermal stability.

According to the data of chemical analysis and nitrogen adsdesorption, as well as the TEM image, clay layers are believed to be important constituents of the walls of the framework pores in sol-PILB−C*n* samples. Considering that both the micelle and the sol particles are positively charged, the formation of mesostructural assembly of the sol particles and surfactants seems to be conflicting in terms of balancing the electrical charges. It is reasonable to expect that the meso-assembly forms with the participation of clay layers that are negatively charged.

This means that the micelles of surfactant molecules form in the galleries between the clay layers surrounded by sol particles and clay layers. In the approach of Galarneau et al.,[13] layered

clays were intercalated with surfactants. TEOS was then allowed to hydrolyze and condense surrounding the surfactants in the galleries. An open-framework of silica formed in the galleries after the removal of the surfactants. An obvious difference in our treatment with surfactants from their approach is that the surfactant was introduced into the system where the sol particles already existed in the interlayer gallery. This should not be a serious obstacle for the surfactant molecules to form micelles in the galleries, if the sol particles are readily to be rearranged. Choy et al.[28] found that the stacking of sol particles within the interlayer space could be rearranged at moderate experimental conditions. It was also reported that when the wet cake of the clay pillared with the sol particles of mixed hydrolysates of silicon and titanium is subjected to a supercritical drying (SCD), a radical change in the framework of the sample occurs.[27] The resultant sample has little micropores because the pillared layered structure in the cake changed to a so-called three-dimensional house of card structure during the SCD process. Besides, we have found that the surfactant treatment and the SCD process do not alter the pillared layered structure in clays pillared with alumina or with mixed oxides of aluminum and lanthanum. These facts suggest that the sol particles in the galleries in the wet cake of the sol-pillared clay can be readily rearranged, and so does the intercalated structure in this clay. The sol particles do not bond the clay layers strongly as other kinds of pillar precursors do. This is a *unique property of the sol particles pillared clays*, which can lead to a variety of pore structures from intercalated clays.

The volume of the wet cake swells accordingly due to the surfactant treatment. Removal of the templates by heat treatment results in the framework mesopores. However, these pores are not as uniform as those in MCM41 samples as indicated by the TEM image and the hysteresis of the nitrogen isotherms for these samples. One possible reason is that part of the wall of the framework mesopores are the clay layers, which results in pores of irregular shapes. The broader pore size distribution for clay sample, compared to that of MCM41, also reflects diversity in the pore geometry of the clay samples.

Role of Titanium. Titanium was introduced to modify the silica sol particles that are originally neutral or negatively charged.[23] Titanium hydroxide sol particles carried positive charges and mixing the two sols results in sol particles of positive charges. They can be intercalated between clay layers by an ion-exchange process. Although sol-PILB and sol-PILB−C*n* samples contain about 9% of TiO_2 (Table 2) no anatase or other crystal phases of TiO_2 was observed on their XRD patterns. This is consistent with the fact that the characteristic FTIR bands in the range 900−600 cm^{-1} for titanium oxide is not observed for sol-PILB and sol-PILB−C*n* samples (Figure 10). According to XRD pattern and FTIR spectra, the anatase phase is found in a bentonite pillared with titanium oxide (Ti−PILB). The pillar precursors for Ti−PILB were obtained also by hydrolysis of titanium tetraisopropoxide, and this Ti pillared clay was calcined at the same conditions as for sol-PILB and its derivatives. The anatase phase is active for photooxidation of organic compounds in water. Ti-PILB is an active catalyst for such a reaction[17] but sol-PILB and sol-PILB−C*n* samples are not.

FTIR spectra also revealed that titanium in sol-PILB and sol-PILB−C*n* samples does not exist in particles of TiO_2 but is dispersed in the silica matrix. This is also evidenced by the presence of Si−O−Ti bonding (the band at about 960 cm^{-1}). The results of DR−UV−vis spectra indicate that Ti atoms may exist in isolated state or partially polymerized through Ti−O−Ti bonding and being highly dispersed among silica in the galleries. Incorporation of titanium into the framework of silica can bring about useful and interesting functionalities to the product clays. The isolated Ti(IV) is regarded as active sites for selective catalytic oxidation of alkanes at moderate conditions.[19] As discussed above, the pore sizes of these clay materials can be tailored by choice of surfactants, which allows us to improve the accessibility of the active sites inside the pores to the reactants molecules significantly. The accessibility has a strong relation with the performance of the catalysts. It would be possible and very desirable to develop efficient oxidation catalysts from these porous clay structures possessing strong active sites and tunable pore structures.

According to the DR−UV−vis results, most of titanium exists in the galleries where the framework mesopores form. This inevitably results in evident differences in the surface composition of the pore walls from pure silica. It is expected, in turn, to bring about substantial difference in the surface property of the samples from that of MCM41 materials.

Surface Chemistry. The water adsorption data have shown that the clay samples have much more hydrophilic and, thus, polar surfaces, compared to MCM41. Usually, the surfaces in calcined pillared clays are found to be hydrophobic.[51,58] This is because the pillar precursors have been converted to oxide particles and protons which were released during the calcination migrated into the clay layers. The surface of the pore walls, i.e., the surface of clay layer, and the oxide particles exhibit weak polarity. Thus, the hydrophilicity of the clay samples in the present study may also be attributed to the existence of titanium. The strong surface polarity of the clay samples is related to the strong acidity of their surface, as reflected by the results of pyridine TPD experiments. In addition to the surface composition, the acidic environment from which the wet cake was obtained is another cause for the strong surface acidity of the clay samples. The sols for the sol-PILB were prepared in very acidic conditions. Even after separation, washing, drying, and calcination, the resultant solid exhibits obvious acidity. The pH of a dispersion of calcined sol-PILB powder in water is about 3.1, even lower than the pH of the dispersion of a calcined alumina pillared clay (4.5). The results of pyridine TPD experiments provide a more quantitative picture that sol-PILB−C*n* samples have a substantial amount of strong acid sites. This property is important when they are used as catalysts and catalyst supports.

Conclusions

Layered clay pillared with a mixed sol of silicon and titanium oxides is a unique class of pillared intercalated layered clays. Treating the wet cake of such sol-pillared clay with surfactants of organic ammonium can create a highly porous clay heterostructure of mainly mesopores. We believe that the surfactant molecules diffuse into the galleries between clay layers and form micelles which act as a template agent, similar to the case in MCM41 preparation. From the point of view of electrical charge balance, surfactant micelles and the sol-particles are favored to form meso-phase assemblies in the galleries between clay layers because the micelles and the sol-particles are positively charged, whereas the clay layers bear negative charges. The removal of the surfactants results in very high porosity in the products and the pore sizes of the samples increase with the length of the carbon chain of the surfactants. In combining approaches of pillaring and templating, we have demonstrated that we could prepare porous clay structures with tailorabe pore structures and high porosity. The pore geometry of the solids thus obtained is

not as uniform as in MCM41. However, they exhibit much stronger surface acidity and hydrophilicity than MCM41 samples. These surface properties could be related to the presence of titanium in the clay samples. The titanium does not form pure titanium oxide phase but highly disperse in the silica matrix in the galleries. Therefore these samples show no catalytic activity for photooxidation of organic compounds in water unlike titania (anatase) pillared bentonite. However, they may be excellent candidates for catalytic oxidation of alkanes into alcohols and ketones under modest conditions because the structure of titanium in them reveals the presence of strong active sites for this reaction. The flexibility in tailoring the pore structure with template agents combining with the surface properties, manifest the sol-derived porous clay heterostrcuture (sol-PILB−C*n*) as very promising candidates as adsorbents and catalysts.

Acknowledgment. Financial supports from the Australian Research Council and the University of Queensland are gratefully acknowledged.

References and Notes

(1) Brindley, G. W.; Semples, R. E. *Clay Miner*. **1977**, *12*, 229.
(2) Lahav, N.; Shani, U.; Shabtai, J. *Clays Clay Miner*. **1978**, *26*, 107.
(3) Vaughan, D. E. W. Lussier, R. J.; Magee, J. S. U.S. Patent 4 176 090, 1979.
(4) Pinnavaia, T. J. *Science* **1983**, *220*, 365−371.
(5) Burch, R., Ed. *Catalysis Today*, *2*; Elsevier: New York, 1988.
(6) Barrer, R. M. *Zeolites and Clay Minerals as Sorbents and Molecular Sieves*; Academic Press: London, 1975.
(7) Clearfield, A.; Kuchenmeister, M. E.; Wade, K.; Cahill, R.; Sylvester, P. *Expanded Clays and Other Microporous Solids*; Occelli, M. L., Robson, H. E., Eds.; Van Norstrand Reinhold: New York, 1992; p 245.
(8) Figureas, F. *Catal. Rev., Sci. Eng*. **1988**, *30*(*3*), 457.
(9) Molinard, A.; Vansant, E. F. *Adsorption* **1995**, *1*, 49.
(10) Kresge, C. T.; Leonowicz, M. E.; Roth, W. J.; Vartuli, J. C.; Beck, J. S. *Nature* **1992**, *359*, 710.
(11) Inagaki, S., Fukushima, Y., Kuroda, K. *J. Chem. Soc. Chem. Commun*. **1993**, 680.
(12) A special issue was published on the subject of mesoporous molecular sieves obtained by the templating approach. *Micropor. Mesopor. Mater*. **1999**, *2*.
(13) Galarneau, A.; Barodawalla, A.; Pinnavaia, T. J. *Nature* **1995**, *374*, 529.
(14) Takahama, K.; Yokoyama, M.; Hirao, S.; Yamanaka, S.; Hattori, M. *J. Ceram. Assoc. Jpn., Int. Ed.* **1991**, *99*, 14.
(15) Gil, A., Gandia, L. M., Vicente, M. A. *Catal. Rev*. **2000**, *42*(1/2) 145.
(16) Mattews, R. W. in *Photocatalytic Purification and treatment of Water and Air*, Ollis, D. F. and Al-Ekabi, H., Eds., Elsevier Science: Lausanne, 1993; p 121.
(17) Linsebigler, A. L.; Lu, G.; Yates, J. T. *Chem. Rev.* **1995**, *95*, 735.
(18) Ding, Z.; Zhu, H. Y.; Lu, G. Q.; Greenfield, P. F. *J. Colloid Interface Sci*. **1999**, *209*, 193.
(19) Bordiga, S.; Coluccia, S.; Lamberti, C.; Marchese, L.; Zecchina, A.; Boscherini, F.; Genoni, F.; Leofanti, G.; Pertrini, G.; Vlaic, G. *J. Phys. Chem.* **1994**, *98*, 4125.
(20) Huybrechts, D. R. C.; De Bruycker, L.; Jacobs, P. A. *Nature* **1990**, *345*, 240.
(21) Clerici, M. G. *Appl. Catal.* **1991**, *68*, 249.
(22) Bellussi, G.; Carati, A.; Clerici, M. G.; Maddinelli, G.; Millini, R. *J. Catal.* **1992**, *133*, 220.
(23) Yamanaka, S.; Inoue, Y.; Hattori, M.; Okumura, F.; Yoshikawa, M. *Bull. Chem. Soc. Jpn.* **1992**, *65*, 2494.
(24) Medlin, J. H.; Suhr, N. H.; Bodkin, J. B. *At. Absorpt. Newsl*. **1969**, *8*, 25.
(25) Gregg, S. J.; Sing, K. S. W. *Adsorption, Surface Area and Porosity*, 2nd ed.; Academic Press: New York, 1982, Chapter 2 and 3.
(26) Lippens, B. C and De Boer, J. H. *J. Catal*. **1965**, *4*, 319.
(27) Occelli, M. L.; Peaden, P. A.; Ritz, G. P.; Iyer, P. S.; Yokoyama, M. *Micropor. Mater.* **1993**, *1*, 99.
(28) Choy, J.-H.; Park, J.-H.; Yoon, J.-B. *J. Phys. Chem. B* **1998**, *102*, 5991.
(29) Brunauer, S.; Demming, L. S.; Demming, W. S.; Teller, E. *J. Am. Chem. Soc*. **1940**, *62*, 1723.
(30) Branton, P. J.; Hall, P. G.; Sing, K. S. W. *J. Chem. Soc. Chem. Commun.* **1993**, 1257.
(31) Franke, O.; Schulz-Ekloff, G.; Rothousky, J.; Stárek, J.; Zukal, A. *J. Chem. Soc. Chem. Commun.* **1993**, 724.
(32) Branton, P. J., Hall, P. G.; Sing, K. S. W., Reichert, H., Schüth, F, Unger, K. K. *J. Chem. Soc. Chem. Faraday Trans.* **1994**, *90*, 2965.
(33) Llewellyn, P. L., Grillet, F.; Schüth, F.; Reichert, H.; Unger, K. K. *Micropor. Mater.* **1993**, *3*, 345.
(34) Zhu, H. Y., Zhao, X. S., Lu, G. Q. and Do, D. D. *Langmuir* **1996**, *12*, 6513.
(35) Kruk, M., Jaroniec, M. and Sayari, A. *J. Phys. Chem. B* **1997**, *101*, 583−589.
(36) Galarneau, A. Desplantier, D., Dutartre, R. Di Renzo, F. *Micropor. Mesopor. Mater.* **1999**, *2*, 297.
(37) Dubinin, M. M. *Progress in Surface and Membrane Science*; Cadenhead, D. A., Danielli, J. F., Rosenberg, M. D., Eds.; Academic Press: London 1975; p 1−71.
(38) Horvath, G., Kawazoe, K. *J. Chem. Eng. Japan* **1983**, *16*(*6*), 470.
(39) Zhu, H. Y.; Lu, G. Q. *Characterization of Porous Solids V;* Unger, K. K., Rouquerol, J., Rodriguez-Reinoso, F., Sing, K. S. W., Eds.; Elsevier Science: Amsterdam, 2000; p 243.
(40) Sing, K. S. W. In *Surface Area Determination, Proc. Int. Symp.*; Everett, D. H., Ottewill, R. H., Eds.; Butterworths: London, 1970; p 25.
(41) Occelli, M. L. *Ind. Eng. Chem. Prod. Res. Dev.* **1983**, *22*, 553.
(42) Zhu, H. Y.; Xia, J. A.; Vansant, E. F.; Lu, G. Q. *J. Porous Mater*. **1997**, *4*, 17.
(43) Farmer, V. C.; Russell, J. D. *Clays & Clay Minerals*; Proc. 15th Conf. Pergamon Press: Oxford, 1968; p 121.
(44) Duran, A.; Serna, C.; Fornes, V.; Fernandez Navarro, J. M. *J. Non-Cryst. Solid* **1986**, *82*, 69.
(45) Mukherjee, S. P. *J. Non-Cryst. Solid* **1980**, *28*, 477.
(46) Bertoluzza, A.; Fagnano, C.; Morelli, M. A. *J. Non-Cryst. Solid* **1982**, *48*, 117.
(47) Decottignies, M.; Phalippou, J.; Zarzycki, J. *J. Mater. Sci.* **1978**, *13*, 2605.
(48) Camblor, M. A.; Corma, A.; Pérez-Pariente, J. *J. Chem. Soc. Chem. Commun*. **1993**, 557.
(49) Blasco, T.; Camblor, M. A.; Corma, A.; Pérez-Pariente, J., *J. Am. Chem. Soc.* **1993**, *115*, 11 806.
(50) Gonzalez-Oliver, C. J. R.; James, P. F.; Rawson, H. *J. Non-Crystal. Solid* **1982**, *48*, 129.
(51) Malla, P. B.; Komarneni, S. *Clays Clay Miner*. **1990**, *38*, 363.
(52) Cveanovic, R. J.; Amenomiya, Y. *Adv. Catal*. **1967**, *17*, 103.
(53) Garbowski, E.; Praliaud, H. *Catalyst Characterization*: *Physical Techniques for Solid Materials*; Imelik, B., Vedrine, J. C., Eds.; Plenum Press: New York, 1994; p 61.
(54) Benjelloun, M.; Cool, P.; Linssen, T.; Vansant, E. F. *Micropor. Mesopor. Mater*. **2001**, *49*(1−3), 83.
(55) Zecchina, A.; Spoto, G.; Bordiga, S.; Ferrero, A.; Pertrini, G.; Leofanti, G.; Padovan, M. *Stud. Surf. Sci. Catal.* **1991**, *69*, 251.
(56) Pertrini, G.; Cesana, A.; De Alberti, G.; Genoni, F.; Leofanti, G.; Padovan, M.; Paparatto, G.; Rofia, P. *Stud. Surf. Sci. Catal.* **1991**, *68*, 761.
(57) Blitz, J. P. In *Modern Techniques in Applied Molecular Spectroscopy*; Mirabella, F. M., Eds.; John Wiley & Son: New York, 1998; p 61.
(58) Zhu, H. Y.; Gao, W. H., Vansant, E. F. *J. Colloid Interface Sci*. **1995**, *171*, 377.